Bulletin of the Seismological Society of America, Vol. 99, No. 4, pp. 2523–2540, August 2009, doi: 10.1785/0120080007

Regional Source Scaling of the 9 October 2006 Underground Nuclear Explosion in North Korea

by Tae-Kyung Hong and Junkee Rhie

Abstract The 9 October 2006 underground nuclear explosion (UNE) test in North Korea was well monitored by dense regional seismic stations in South Korea, Japan, and China. This observation allows extensive investigation of the regional source properties of the UNE. The moment for isotropically radiated energy from the UNE is estimated to be 2.92×10^{14} N m. Source spectra of major regional phases from the UNE are studied by inverting for apparent moments, corner frequencies, overshoot parameters, attenuation factors, and frequency power-dependence parameters. The overshoot parameters of P phases from the UNE are estimated to be high, while those of S phases are estimated to be significantly low. The inverted source spectra agree well with conventional models. The low overshoot parameters of S phases suggest that their excitation sources may be different from those for Pn and Pg. It is shown that Pn/Lg and Pg/Lg amplitude ratios are useful for discriminating between UNEs and natural earthquakes in the frequencies of 1–8 Hz.

Introduction

The shear-wave excitation mechanism from an underground nuclear explosion (UNE) has not yet been fully understood, despite various efforts. This is partly because UNEs have been recorded by sparse local or regional seismic stations due to geographical and political limitations (e.g., Peppin, 1976; Hong and Xie, 2005; Fisk, 2007). The sparse observation of UNEs prevents thorough investigation of regional source properties (cf, Murphy and Barker, 2001). The source properties could be partly understood through statistical analyses of various sparse UNE records (e.g., Xie and Patton, 1999; Al-Eqabi *et al.*, 2001; Fisk, 2006). However, many aspects of UNE source properties still remain unclear.

In the inversion of source spectra from regional waveforms, a theoretical source spectral model should be adopted. Several UNE source spectral models have been proposed (e.g., Mueller and Murphy, 1971; Aki *et al.*, 1974; Lay *et al.*, 1984; Sereno *et al.*, 1988; Denny and Johnson, 1991). These UNE source spectral models incorporate overshoot parameters for the description of characteristic spectral amplification around the corner frequencies (Aki *et al.*, 1974; Lay *et al.*, 1984). It is known that the overshoot parameter and corner frequency vary with source depth and source-region properties (Mueller and Murphy, 1971; Lay *et al.*, 1984; Fisk, 2007). However, the overshoot feature has not been examined sufficiently for various types of UNEs.

Various techniques have been proposed for discriminating nuclear explosions from natural earthquakes (Stevens and Day, 1985; Woods *et al.*, 1993; Kim *et al.*, 1997; Xie and Patton, 1999). One promising method is to compare Pn/Lg spectral amplitude ratios between UNEs and earthquakes. This method requires us to analyze source spectra of the UNE and a nearby earthquake because regional waveforms can vary with ray paths.

The 9 October 2006 nuclear explosion in North Korea was recorded by dense regional networks in China, Japan, and South Korea. This UNE test in North Korea provides us a valuable chance to investigate the regional source properties. We invert for source parameters of regional phases, and examine the characteristics of P/S spectral amplitude ratios.

Data and Geology

Dense seismic networks are operated in China, Japan, and South Korea (Fig. 1). The 9 October 2006 nuclear explosion test in North Korea was well observed by the regional seismic networks. The magnitude of the event is m_b 4.2 (e.g., Hong *et al.*, 2008). We collect 48 broadband seismic records from the regional networks. The discrete sampling rates of seismometers are 0.05, 0.0125, and 0.01 sec, and the epicentral distances are 307–1116 km. We clearly observe major regional phases (Fig. 2). The azimuths of the UNE to stations in Japan and South Korea are 65°–228°, which is reasonably good coverage considering the azimuthally symmetric radiation pattern of a point source. An additional station, MDJ, is available in the azimuthal direction of 5°.

Seismic records for a nearby earthquake are additionally analyzed for comparison with the UNE. The earthquake

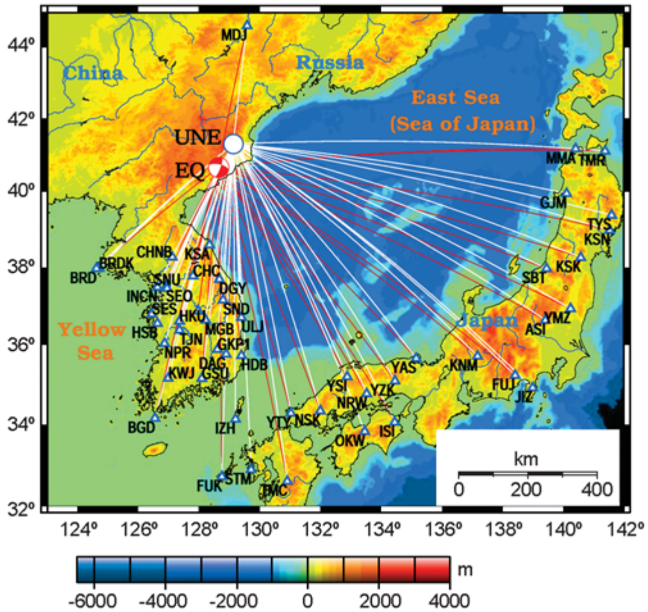

Figure 1. Map of events and stations. The locations of the 9 October 2006 UNE (on the map) and a nearby m_b 4.1 earthquake on 16 April 2002 (EQ) are marked with circles. The deviatoric moment tensor solution of the earthquake is presented. Both events were well observed by dense regional networks deployed in China, Japan, and South Korea (triangles). The great-circle paths are marked with solid lines.

occurred at ~82 km southwest from the UNE on 16 April 2002 (Fig. 1). The focal depth is 10 km and the magnitude is m_b 4.1 according to the bulletin of the International Seismological Center (see Data and Resources section). Note that the northeastern part of the Korean Peninsula is a seismologically quiescent place, and the earthquake is the only one with magnitude greater than 4.0 since 2000. The waveform variation of the earthquake with distance is similar to that of the UNE. High-frequency regional waves from both events are well observed in the stations (Fig. 2b,d).

The area of the Korean Peninsula has experienced complex tectonic evolutions including continental collision and rifting (Chough *et al.*, 2000). The continental rifting caused the opening of the East Sea (Sea of Japan) between Korea and Japan. Thus, the region around the east coast of the southern Korean Peninsula consists of the continental margin in which the crustal structure changes abruptly with distance from the coast (Cho *et al.*, 2004). Crustal phases are significantly attenuated across the continental margin (Hong *et al.*, 2008).

Moment from Long-Period Waveform Inversion

We analyze long-period waveforms to estimate the moments of the UNE and the earthquake. Long-period waves are less sensitive to small-scale structure along ray paths than short-period waves. We analyze seismic records of stations MDJ, CHC, and SNU (Fig. 1) considering the signal-to-noise levels and azimuthal coverage. Their epicentral distances are less than 470 km.

The isotropic moment of the UNE is estimated using a long-period waveform inversion technique (Dreger and Helmberger, 1993). The choice of a frequency band sustaining sufficiently large signal-to-noise level is crucial for stable inversion. We examine spectral contents of waveforms relative to those of background noises before the *Pn* onset time. The spectral amplitude ratios between the signal and noise are presented in Fig. 3. We find that the signal-to-noise ratio is sufficiently large in the frequency range between 0.05 and 0.16 Hz.

We analyze waveforms band-pass-filtered between 0.05 and 0.1 Hz for the long-period waveform inversion. Note that the regional waves with dominant frequency around 1 Hz are significantly influenced by crustal structures, while long-period waves are less influenced by small-scale crustal variations (e.g., Hong *et al.*, 2008). Thus, long-period waveform inversions can be performed stably with an average velocity model. We apply the 1D seismic velocity model of Chang and Baag (2005) for the inversion.

The seismic waveforms from a source can be expressed by (Aki and Richards, 1980, p 53)

$$A_j(\mathbf{x}_i, \mathbf{x}_s, t) = M_{pq}(t) * G_{jp,q}(\mathbf{x}_i, \mathbf{x}_s, f_0, t) + E_j(\mathbf{x}_i, \mathbf{x}_s, t), \tag{1}$$

where $A_j(\mathbf{x}_i, t; \mathbf{x}_s, 0)$ is the observed displacement time record in component j of station i at $\mathbf{x}_i$ for a source located at $\mathbf{x}_s$, $M_{pq}(t)$ is the moment tensor with source-time function, $G_{jp}(\mathbf{x}_i, \mathbf{x}_s, f_0, t)$ is the Green's function corresponding to the displacement in j component at station i for a point impulse of frequency f_0 in the direction of p, and $G_{jp,q}$ is the Green's function differentiated in the spatial direction of q. In addition, $E_j^i(t)$ is the error term accounting for the non-double-couple component of the source and incorporation of an imperfect Green's function. Here, the source-time function of an event can be disregarded for expression of long-period displacements because regional seismic waves are dominated by short-period energy.

The moment tensor of an event can be described with a sum of isotropic and deviatoric components (Ford *et al.*, 2008):

$$M_{ij} = M_{ij}^{\mathrm{iso}} + M_{ij}^{\mathrm{dev}}, \qquad i, j = 1, 2, 3, \tag{2}$$

where M_{ij}^{iso} is

$$M_{ij}^{\mathrm{iso}} = \delta_{ij}(M_{11} + M_{22} + M_{33})/3, \tag{3}$$

and M_{ij}^{dev} is

$$M_{ij}^{\mathrm{dev}} = M_{ij} - \delta_{ij}(M_{11} + M_{22} + M_{33})/3. \tag{4}$$

Here, an explosive source is dominated by the isotropic component (M_{ij}^{iso}), and a double-couple source is dominated by

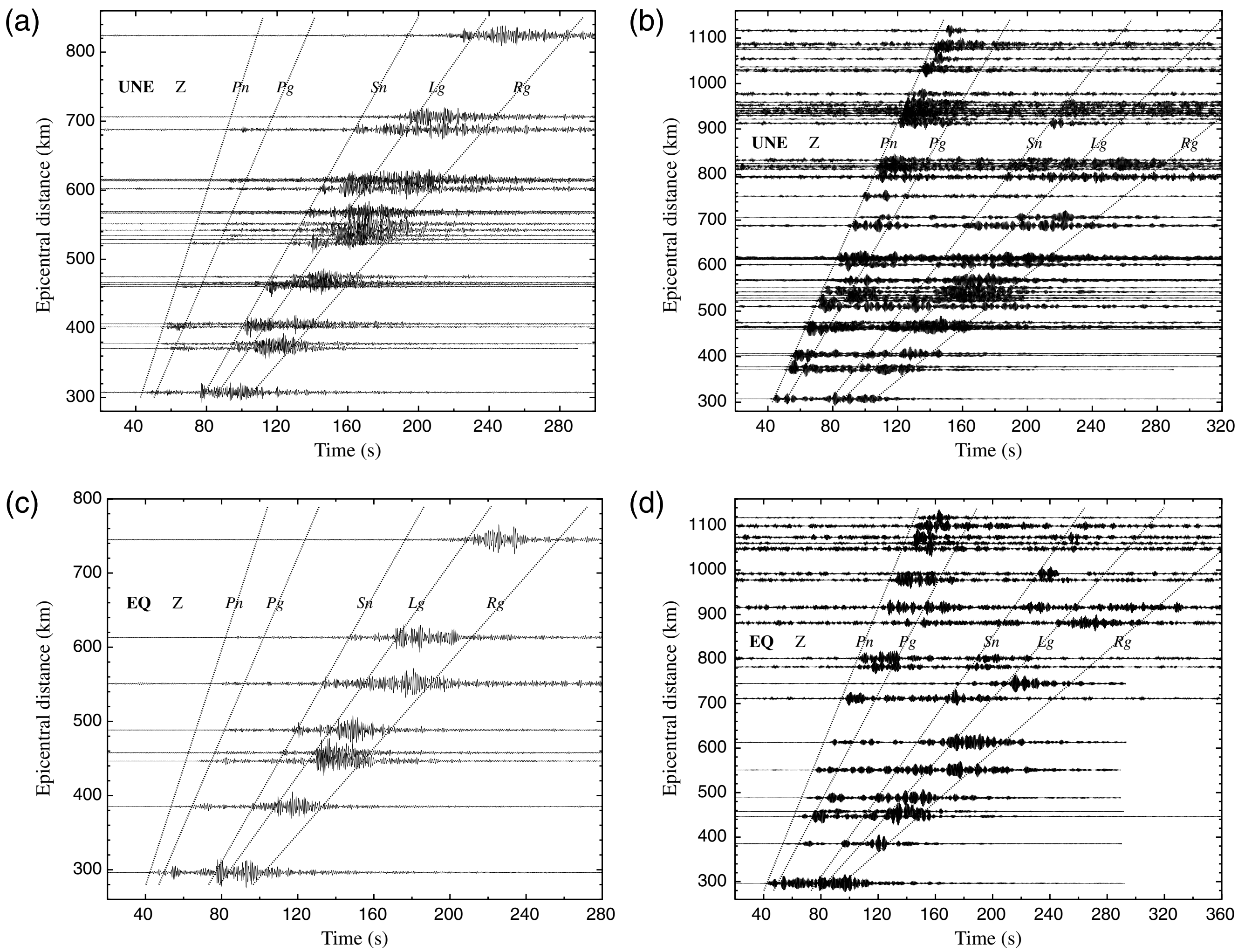

Figure 2. Vertical velocity seismograms of the UNE (a, b) and earthquake (c, d). The seismograms in the left column are band-pass-filtered between 1 and 2 Hz, and those in the right column are 2 Hz records. The major regional phases (*Pn*, *Pg*, *Sn*, and *Lg*) are denoted. The phase velocities of travel-time curves for *Pn*, *Pg*, *Sn*, and *Lg* are 7.95, 6.05, 4.5, and 3.57 km/sec, respectively. Phase *Rg* with apparent velocity of 2.9 km/sec is barely detectable. High-frequency *P* phases are observed up to a distance of 1100 km.

the deviatoric component (Ford *et al.*, 2008). We measure the isotropic moment for the UNE and the deviatoric moment for the earthquake.

The Green's functions for an explosive source and a double-couple source are computed using a frequency-wavenumber integration method (Saikia, 1994). We then align the observed waveforms with the synthetic Green's function using cross correlations to correct for unmodeled complex 3D propagation effects. We use vertical and radial components for the UNE waveform inversion, counting only the isotropic radiation component. The UNE waveform inversion based on equation (1) is an overdetermined problem with only one unknown (M_0^{iso}). The 200 sec waveforms around the maximum amplitudes in the time records are analyzed for the waveform inversion. We estimate the deviatoric moment tensor (M_0^{dev}) of the earthquake using three-component records.

The isotropic moment of the UNE is estimated to be 2.92×10^{14} N m. The deviatoric moment of the earthquake is given by 1.42×10^{14} N m. The inverted moment tensor solution is presented in Figure 1. The variance reduction is 62% in the UNE waveform inversion and 71% in the earthquake waveform inversion. The focal depth of the earthquake is estimated to be 7 km, which reasonably agrees with the Bulletin of the International Seismological Center (10 km).

Note that the estimated isotropic moment of the UNE is consistent with Walter *et al.* (2007), which estimated the UNE moment by 3×10^{14} N m. This isotropic moment estimate corresponds to an m_b of 4.12–4.66 according to the regional moment-magnitude relationship of Patton and Walter (1993). This inferred body-wave magnitude agrees well with the recent m_b estimate of Hong *et al.* (2008). When the isotropic moment is inverted for each station, the mean isotropic moment is estimated to be 2.97×10^{14} N m with a standard deviation of 0.57×10^{14} N m. The synthetic waveforms for both the UNE and the earthquake agree well with the observed waveforms for all stations (Fig 4).

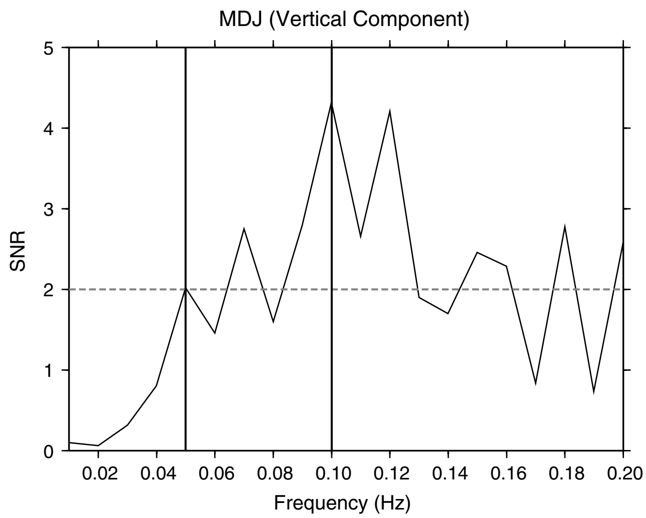

Figure 3. Signal-to-noise ratio (SNR) of a vertical seismogram of station MDJ as a function of frequency. Time records before *P* onset time are analyzed for background noises, and those after *P* onset time are for signals from UNE. The length of the time window is 100 sec. Two vertical solid lines indicate the low and high ends of the frequency band applied for the waveform inversion.

Theoretical Source Spectral Model

The waveform of a phase is the result of the combined influence of source and ray path properties. The amplitude of a phase can be expressed by (Sereno *et al.*, 1988; Taylor and Hartse, 1998; Xie and Patton, 1999)

$$A_i(f) = S(f)G(d_i)\exp\left[-\frac{\pi f d_i}{v_g Q_i(f)}\right]e_i(f), \tag{5}$$

where $A_i(f)$ is the ground motion at station i at the frequency of f, $S(f)$ is the source spectrum, $G(d_i)$ is the geometrical spreading term for the distance of d_i, $Q_i(f)$ is the attenuation factor for the ray path to station i, v_g is the group velocity of the phase, and $e_i(f)$ is the cumulative effect of the other minor factors along the ray path.

The UNE source spectrum $S(f)$ in (5) can be expressed by (Mueller and Murphy, 1971; Sereno *et al.*, 1988; Xie and Patton, 1999)

$$S(f) = \frac{M_0}{4\pi\rho_s v_s^3\sqrt{1+(1-2\xi)f^2/f_c^2+\xi^2 f^4/f_c^4}}, \tag{6}$$

where M_0 is the moment, ξ is the overshoot parameter, f_c is the corner frequency, ρ_s is the density in the source region, and v_s is the velocity of the phase in the source region. The quality factor for the ray path to station i can be expressed as a function of frequency

$$Q_i(f) = Q_{0,i}f^{\eta_i}, \tag{7}$$

where $Q_{0,i}$ is the quality factor at 1 Hz and η_i is the power-law frequency dependence term. The frequency-independent geometrical spreading factor is given by

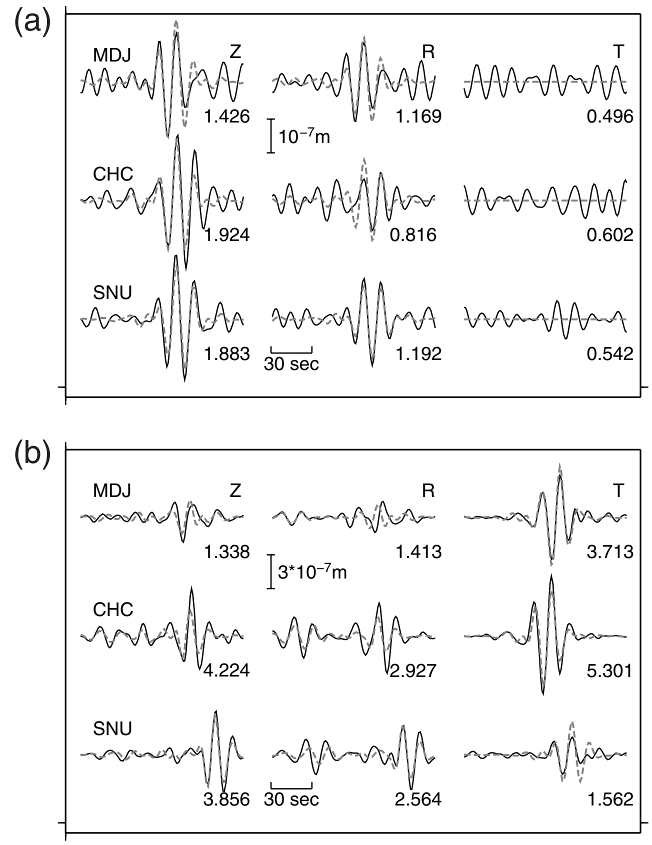

Figure 4. Comparison of displacement waveforms between observed (solid) and synthetic (dotted gray) seismic records for stations MDJ, CHC, and SNU: (a) the UNE in North Korea, and (b) the nearby m_b 4.1 earthquake. A band-pass filter between 0.05 and 0.1 Hz is applied. Moment tensors are calculated by time domain waveform inversions. Synthetic waveforms are computed using the isotropic moment tensor for the UNE and the deviatoric moment tensor for the earthquake. The maximum amplitudes in the unit of 10^{-7} m are denoted.

$$G(d_i) = (d_0/d_i)^{\gamma}d_0^{-1}, \tag{8}$$

where γ is the decay rate of phase and d_0 is the reference distance.

Note that the UNE source spectral model was originally developed for the description of compressional waves (Mueller and Murphy, 1971). In this study we apply this model for source spectral inversion of *S* phases to investigate the nature of the *S* phases from UNE. We set $d_0 = 100$ km

Table 1
Inverted Corner Frequencies of Regional Phases from the 16 April 2002 Earthquake*

Phase	f_c (Hz)
Pn	5.7
Pg	4.7
Sn	3.0
Lg	2.1

*Has the deviatoric moment M_0 of 1.42×10^{14} N m.

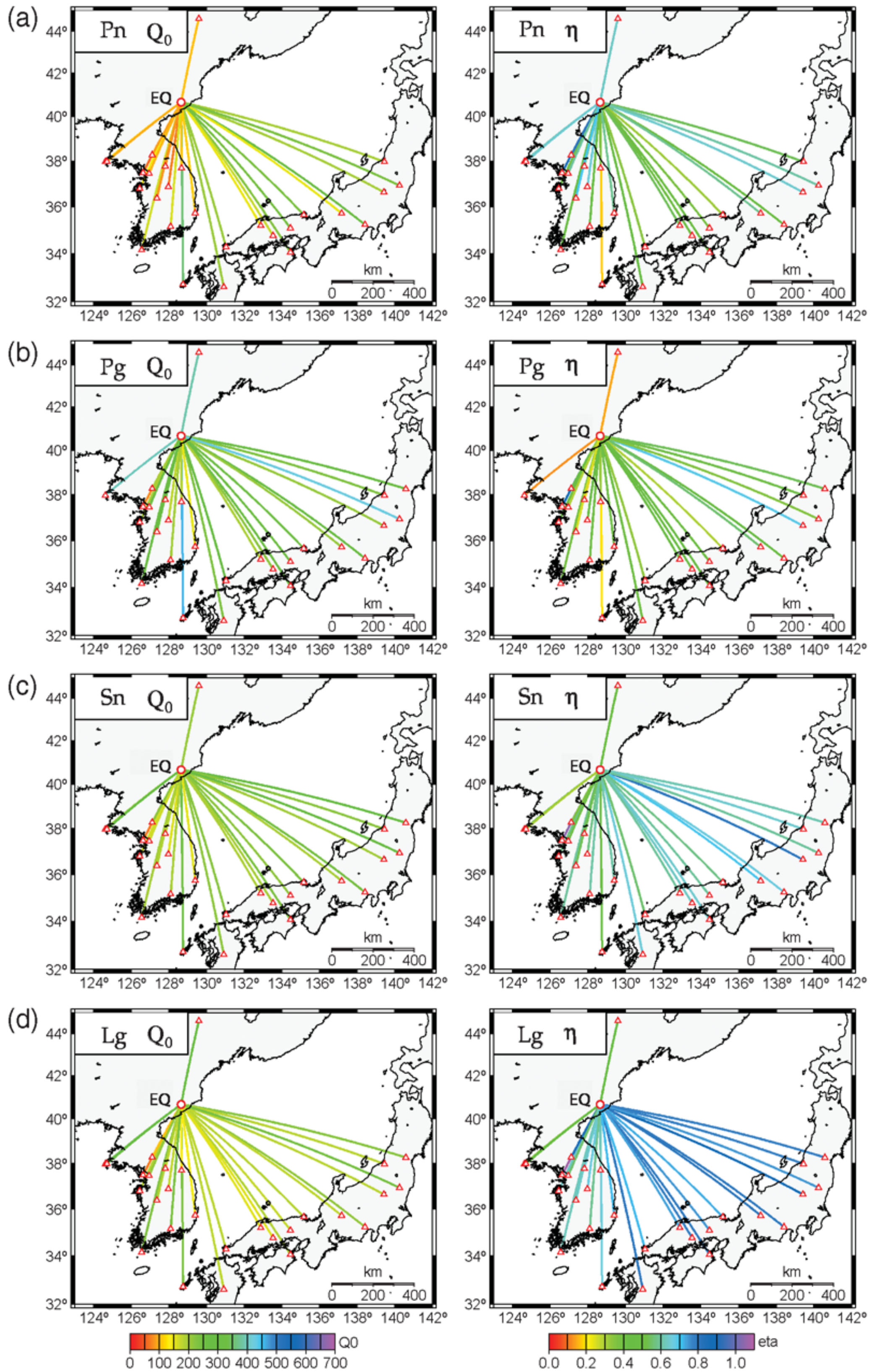

Figure 5. The quality factors at 1 Hz (Q_0) and their frequency power-law dependence terms (η) inverted from the earthquake records: (a) Pn, (b) Pg, (c) Sn, and (d) Lg. The quality factors at 1 Hz are low on ray paths to southern Korea, while those on the other paths are estimated to be relatively high.

Table 2
Inverted Source Spectral Parameters of the 9 October 2006 UNE in North Korea

Phase	M_0 (N m)	f_c (Hz)	ξ
Pn	1×10^{14}	5.1	1.3
Pg	8×10^{13}	5.4	1.0
Sn	4×10^{13}	4.0	0.3
Lg	4×10^{13}	0.9	0.1

and $\gamma = 0.5$ for Lg, and $d_0 = 1$ km and $\gamma = 1.1$ for Pn, Pg, and Sn (Zhu *et al.*, 1991; Walter and Taylor, 2002).

The seismic moment can be measured from the zero-frequency level of source spectrum, which requires an analysis of long-time record sections in practice. In this study we analyze the waveforms of regional phases, which practically have limited time durations. Such limitation of time-window length is inevitable for analyses of regional phases. Thus, it is difficult to estimate the correct moment of event from regional phases.

We invert for the apparent moment, corner frequency, overshoot parameter, and quality factors at 1 Hz and power-law frequency dependence terms from displacement spectra. The model vector to be determined can be written by

$$\mathbf{m}^T = (M_0, f_c, \xi, Q_{0,1}, \eta_1, Q_{0,2}, \eta_2, \cdots, Q_{0,n}, \eta_n)^T, \quad (9)$$

where n is the number of stations. Unknowns M_0, f_c, and ξ are determined using a grid search scheme in the inversion. We compose discrete sets of M_0, f_c, and ξ.

The source spectrum of an earthquake can be expressed by (Brune, 1970; Aki and Richards, 1980, p. 424; Stevens and Day, 1985)

$$S(f) = \frac{M_0 R_{\theta\phi}}{4\pi\sqrt{\rho_s \rho_r v_s^5 v_r}(1 + f^2/f_c^2)}, \quad (10)$$

where $R_{\theta\phi}$ is the amplitude scaling for the radiation pattern, and ρ_r and v_r are the density and seismic velocity in the receiver region, respectively. The radiation pattern $R_{\theta\phi}$ is calculated considering the distribution of stations. We apply $R_{\theta\phi} = 0.63$ for P phases (Pn, Pg) and $R_{\theta\phi} = 0.43$ for S phases (Sn, Lg).

Processing

For analysis of each regional phase, we apply a 4.5 sec long moving time window with 0.2 sec long cosine tapering at both ends (Xie, 2002). The discrete time-shifting interval of the window is equal to the sampling interval of the record. We analyze major regional phases, Pn, Pg, Sn, and Lg. Waveforms in the time range between $d_i/7.95 + 5$ and $d_i/6.6 + 0.8$ sec, where d_i is the epicentral distance in kilometers to station i, are processed for Pn. Waveforms in the time range between $d_i/6.05 + 0.8$ and $d_i/5.0 + 11$ sec are processed for Pg. The time range for Sn is $d_i/4.5 + 11$ to $d_i/3.7 + 0.5$ sec. Waveforms in the times of group velocities between 3.57 and 3.15 km/sec are analyzed for Lg. The average power spectrum between 0.5 and 10 Hz is analyzed. The average power spectra are resampled by a 0.01 Hz interval using a cubic spline interpolation.

We apply velocities of phases, v_g in equation (5), by 7950 m/sec for Pn, 6050 m/sec for Pg, 4550 m/sec for Sn, and 3500 m/sec for Lg considering the seismic velocity structures in the area of the Korean Peninsula (Ritzwoller *et al.*, 2002; Chang and Baag, 2005; Pei *et al.*, 2007). The P- and S-wave velocities in the source and receiver regions (v_s and v_r in equations 6 and 10) are set to be 5670 m/sec and 3273 m/sec. The density in the source region (ρ_s) is 2580 kg/m^3. We deconvolve the instrument responses from the regional waveforms before the source spectral inversion.

We invert the observed spectra for the model parameters in equation (9). Discrete sets of M_0, f_c, and ξ are iteratively applied for an inversion of $Q_{0,i}$ and η_i. Due to the nonuniqueness of inversion, various sets of model parameters can satisfy the observed spectra. For instance, there are trade-offs between Q and M_0. When a high Q is estimated, a low M_0 is determined accordingly and vice versa. Note that both M_0 and Q control the amplitude of the source spectrum. This nonunique determination of Q and M_0 is partly due to analysis of spectra in limited frequency bands. The regional waveform spectra are typically dominated by energy with frequencies of 1–8 Hz. The analysis with narrow spectrum bands may cause unstable estimation of Q and M_0 in the inversion. Model parameters Q_0 and η reflect the properties of ray paths, which are independent from the source properties. Thus, we find that model parameters f_c and ξ are determined stably despite the trade-off between M_0 and Q.

We introduce a two-step inversion scheme. In the first step of the inversion we calculate a set of model parameters with the minimum error. In this step we determine parameters f_c and ξ. In the second step we apply the f_c and ξ that are determined in the first step and determine the other model parameters, M_0 and Q. Model parameters M_0 and Q are determined nonuniquely in the second-step inversion because one parameter is subject to vary with the other parameter. We perform a grid search of moment that yields attenuation factors agreeing with results from other studies. This two-step approach constrains the model parameters easily and helps us to avoid local minima in the inversion. For each inversion we apply the LSQR method (the sparse linear equations and sparse least-squares method; Paige and Sauders, 1982).

Regional seismic waves of frequencies around 1 Hz are highly influenced by crustal structure (Kennett, 1986; Zhang and Lay, 1995; Kennett and Furumura, 2001; Hong *et al.*, 2008). The quality factors (Q_0) are estimated to be stable in the continental region, while those on tectonic margins can vary with ray path due to abrupt variations in crustal structures. The tectonic structures around the Korean Peninsula are complex (Chough *et al.*, 2000), and high

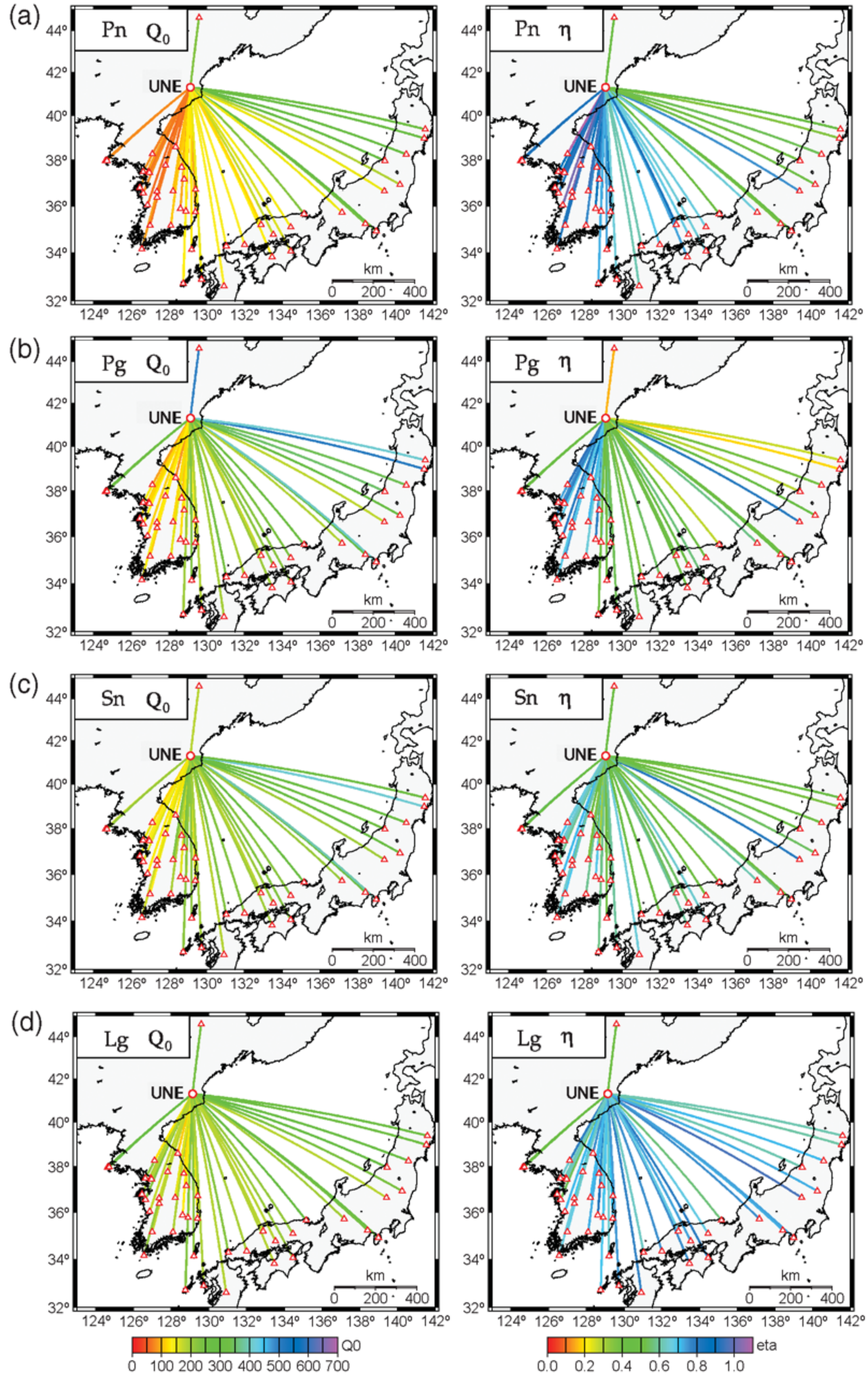

Figure 6. The quality factors at 1 Hz (Q_0) and their frequency power-law dependence terms (η) inverted from the UNE records: (a) Pn, (b) Pg, (c) Sn, and (d) Lg. The P phases display high η on the ray paths to southern Korea and southern Japan but low η to northern Japan.

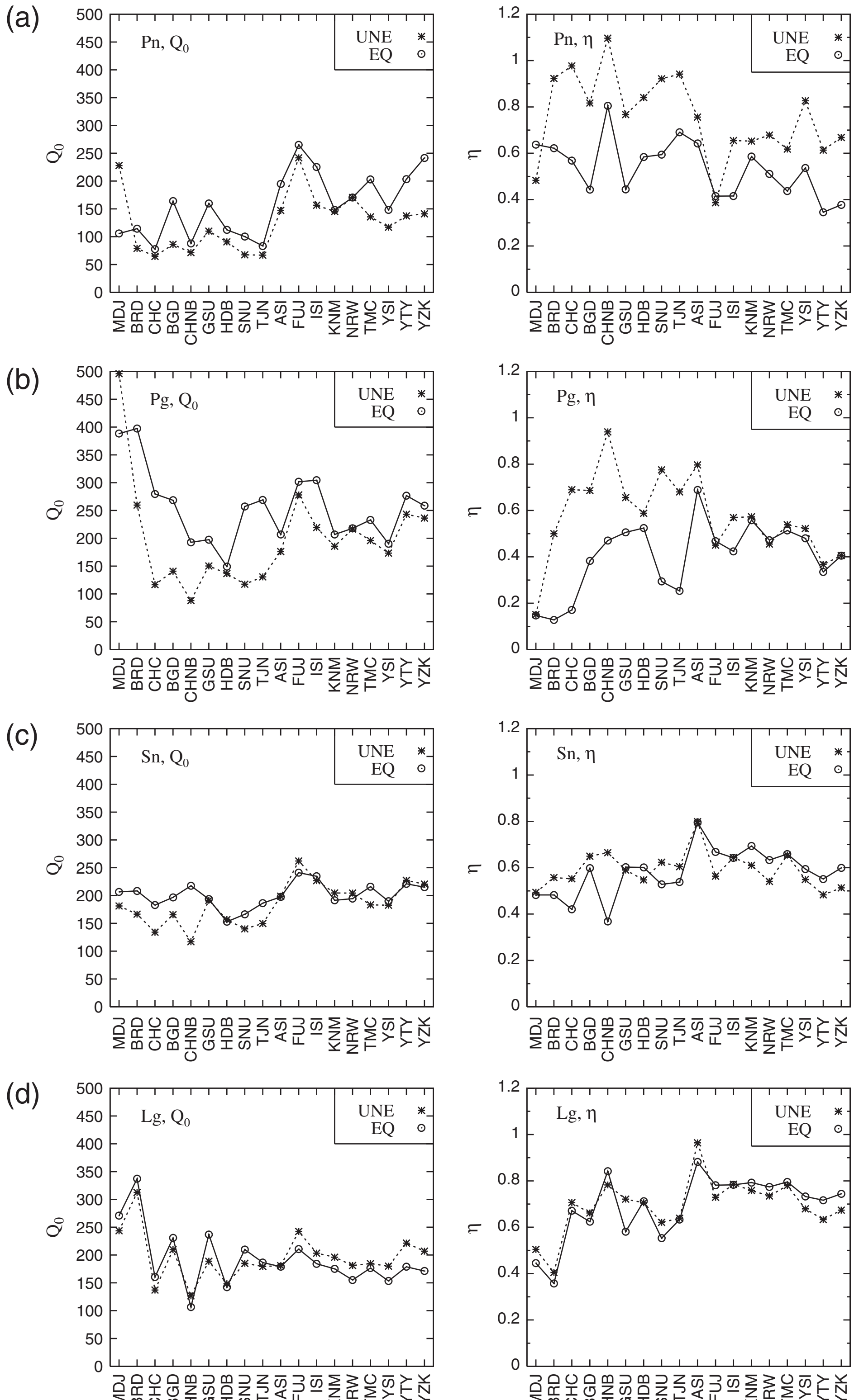

Figure 7. Comparison of Q_0 and η for (a) Pn, (b) Pg, (c) Sn, and (d) Lg phases between the UNE and the earthquake. The Q_0 and η are the quality factor at 1 Hz and the power-law frequency dependence term for ray paths to the stations, respectively. The Q_0 and η of the stations recording both events are presented. The stations names are annotated on the horizontal axis. Station MDJ is located in China, stations BRD–TJN are in South Korea, and stations ASI–YZK are in Japan. The S phases (Sn, Lg) display very similar path parameters between the UNE and the earthquake, while the P (Pn, Pg) phases show some difference by station.

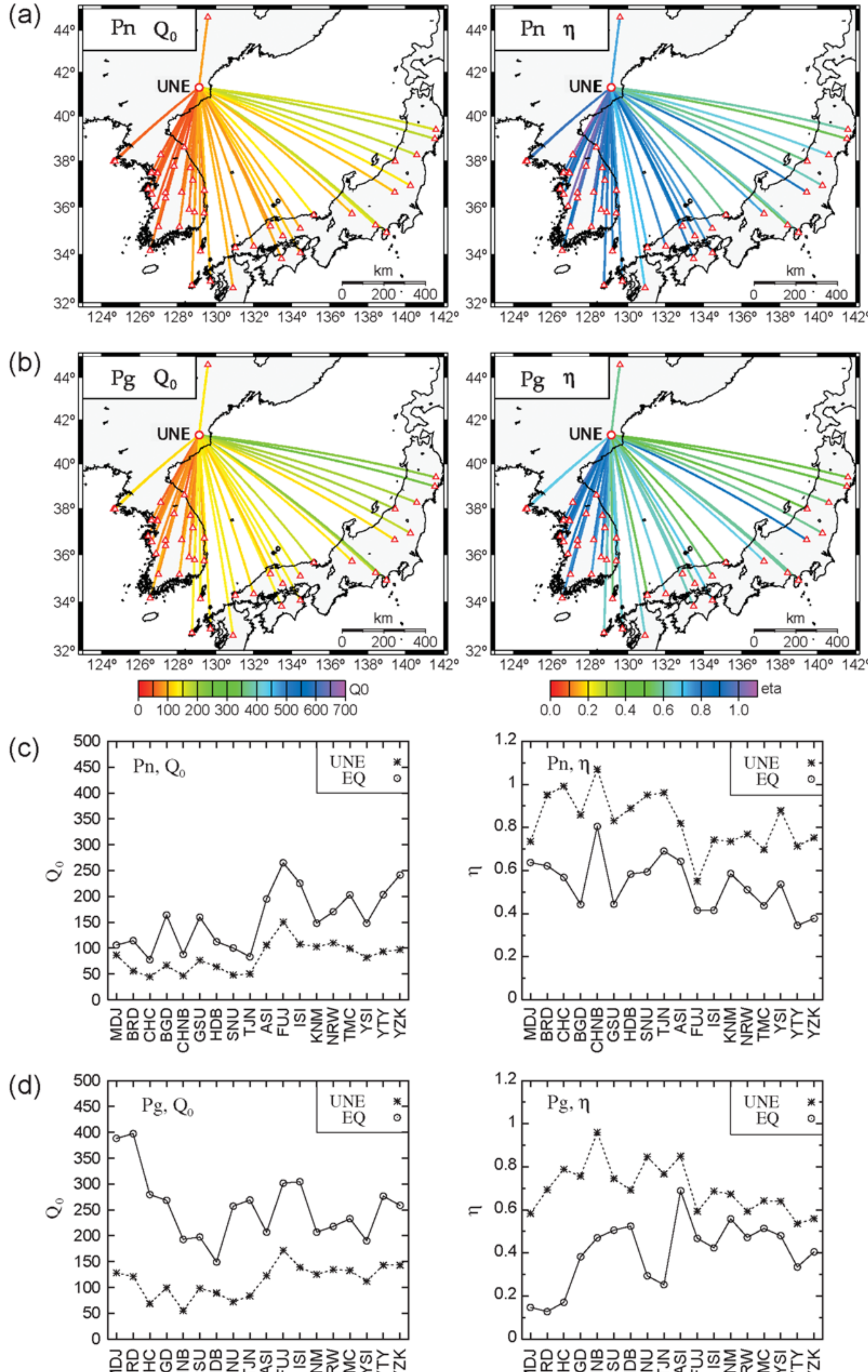

Figure 8. Path parameters of (a) *Pn* and (b) *Pg* for source spectral inversions with implementation of a given moment, 2.92×10^{14} N m, which is obtained from the long-period moment inversion. Comparison of the path parameters with those of the earthquake is also presented ([c] *Pn* and [d] *Pg*). The discrepancy of the inverted path parameters between the UNE and the earthquake becomes increased in both *Pn* and *Pg* phases.

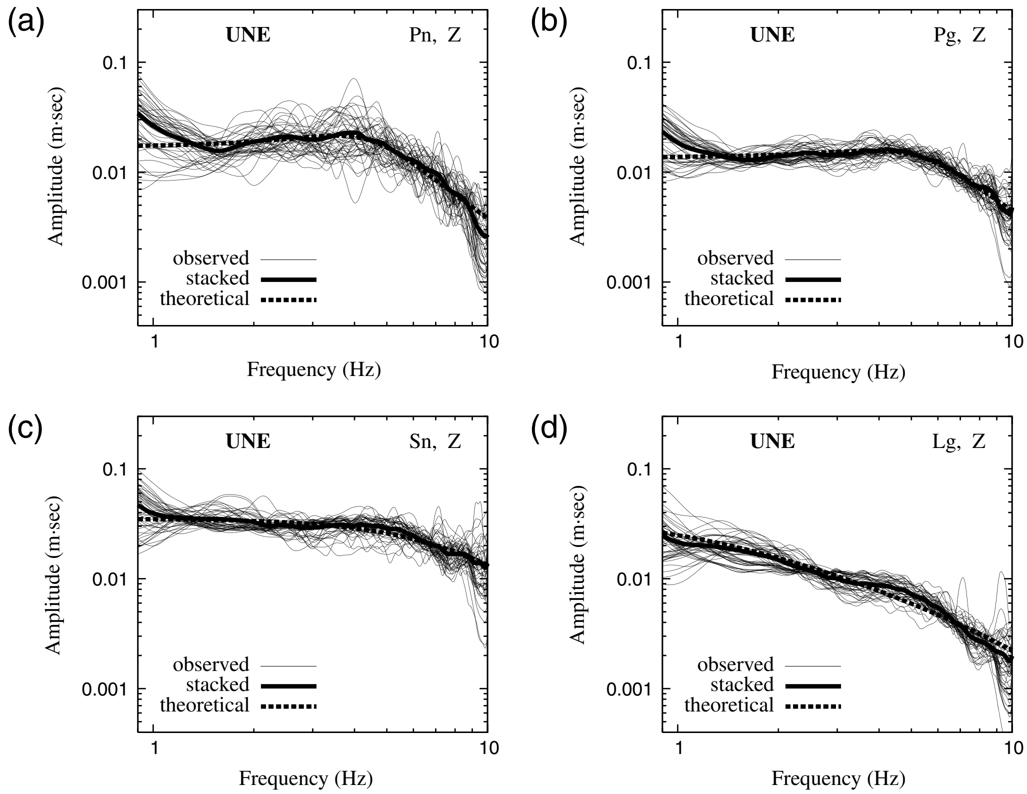

Figure 9. Source spectra of the major regional phases from the UNE: (a) *Pn*, (b) *Pg*, (c) *Sn*, and (d) *Lg*. Vertical-component records are analyzed. The *P* phases display characteristic overshoot features. The *S* phases decrease monotonically with frequency. Inverted source spectra at all stations are drawn with thin lines, and the stacked result is presented with a thick line. Theoretical source spectra are presented with dotted lines. The inverted source spectra agree well with the theoretical curves.

variation of Q is expected. The Lg is the only regional phase that has been studied for the Korean Peninsula (Chung *et al.*, 2007). Seismic attenuation were studied limitedly using local P and S waves for some local areas in the peninsula (Kim *et al.*, 1999; Chung and Sato, 2001). However, the Q distribution of Pn, Pg, and Sn have not been studied. Thus, we directly determine the attenuation factors of regional phases in the source spectral inversion for the 16 April 2002 earthquake by applying the moment determined from the low-frequency waveform inversion. The calculated attenuation factors are used as the existing reference Q for the Q comparison in the two-step source spectral inversion of the UNE.

Inversion of Source Spectral Parameters

We first determine the source parameters of the earthquake. The corner frequencies (f_c) are estimated to be 5.7 Hz for Pn, 4.7 Hz for Pg, 3.0 Hz for Sn, and 2.1 Hz for Lg (Table 1). As we have discussed in the previous section, we apply the moment ($M_0 = 1.42 \times 10^{14}$ N m) determined from the low-frequency waveform inversion and determine unique attenuation factors (Q) along ray paths. The inverted attenuation factors are presented in Figure 5. These attenuation factors are used as the reference Q for comparison with those from the UNE source spectral inversion.

We now determine the source parameters of the UNE. The Pn source spectrum of the UNE is well represented by $M_0 = 1 \times 10^{14}$ N m, $f_c = 5.1$ Hz, and $\xi = 1.3$. The Pg spectrum has M_0 of 8×10^{13} N m, f_c of 5.4 Hz, and ξ of 1.0. For Sn, $M_0 = 4 \times 10^{13}$ N m, $f_c = 4.0$ Hz, and $\xi = 0.3$. For Lg we have $M_0 = 4 \times 10^{13}$ N m, $f_c = 0.9$ Hz, and $\xi = 0.1$ (Table 2).

The estimated Pn overshoot parameter of the UNE is greater than the value conventionally assumed (1.0; Xie and Patton, 1999). On the other hand, the estimated Lg overshoot parameter is significantly lower than the conventional value (0.75; Xie and Patton, 1999). The estimated apparent moments for P phases (Pn, Pg) are about one third of the moment determined from the low-frequency waveform inversion. This may be because the UNE source spectral model may underrepresent the low-frequency content of the UNE spectra.

From the $M_0 - f_c$ scaling relationship of Xie (2002), the corner frequencies of Pn and Lg phases from the earthquake have 8.0 ($\pm$4) and 1.8 ($\pm$0.5) Hz, and those of the UNE have 6.6 ($\pm$3.1) and 1.5 ($\pm$0.3) Hz for the moment estimates from the long-period waveform inversions. The Pn and Lg corner frequencies of this study reasonably agree

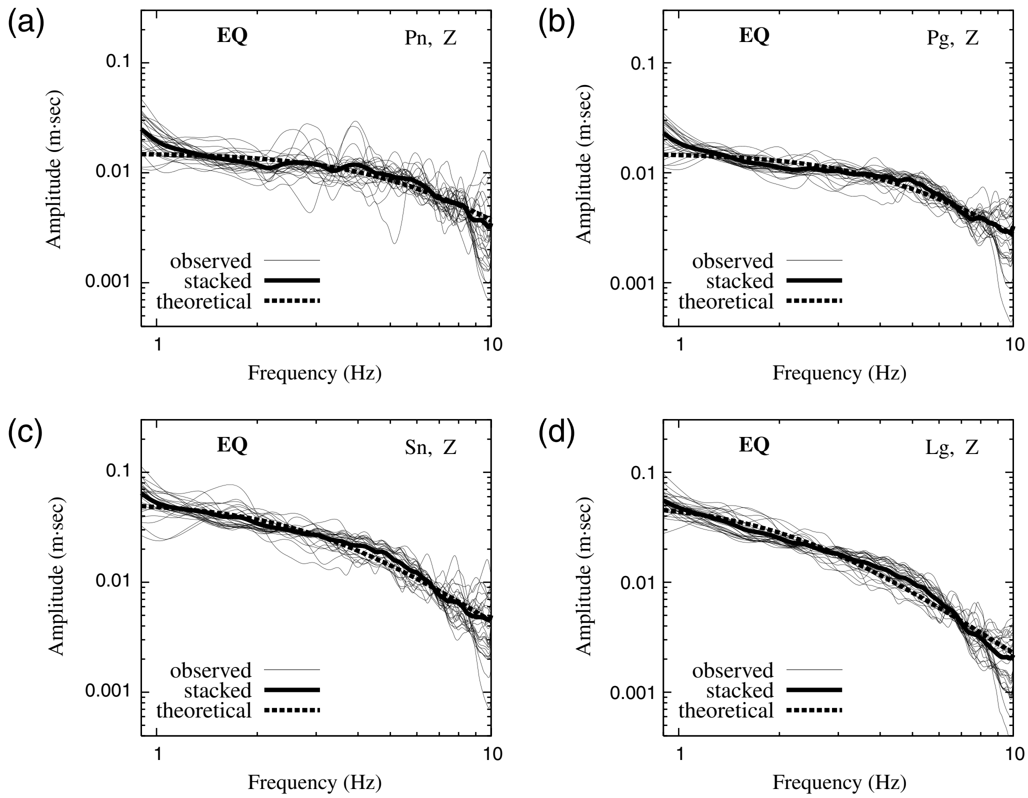

Figure 10. Source spectra of the major regional phases from the earthquake: (a) *Pn*, (b) *Pg*, (c) *Sn*, (d) *Lg*. The observed source spectra agree well with the theoretical curves.

with the scaling relationship of Xie (2002), although the *Lg* from the UNE appears to have a slightly lower corner frequency than the expected value.

The calculated Q_0 and η for the UNE records are presented in Figure 6. The overall distribution of quality factors (Q_0) and power-law frequency dependence terms (η) are similar between the UNE and earthquake, although ray paths from the UNE to the southern Korean Peninsula display much lower Q_0 and higher η than those from the earthquake (Figs. 5–7).

We find characteristic discrepancy in path parameters of *P* phases (*Pn*, *Pg*) between the UNE and the earthquake. The inverted path parameters show that *P* phases from the UNE appear to experience more attenuation at 1 Hz, but less in high frequencies than those from the earthquake. Also, the apparent moments for the *P* phases appear to be smaller than the moment estimate (2.92×10^{14} N m) from long-period inversion. Note that the source spectral model of UNE in equation (6) was originally developed for compressional waves (Mueller and Murphy, 1971). Thus, we additionally conduct source spectral inversions of the *P* phases with a given moment of the moment estimate from long-period moment inversion.

We find that the discrepancy in path parameters is increased although the corner frequencies and overshoot parameters are hardly changed (Fig. 8). These observations confirm that the apparent moments for the *P* phases are smaller than the moment estimate from the long-period asymptote. This may be because the source spectral amplitude level of the UNE is not simply constant in low-frequency regimes, unlike the expectation in the source spectral model.

The apparent difference in Q_0 and η of *P* phases between the UNE and the earthquake may be explained with source properties and/or wave responses to medium, which may include: (1) inaccurate representation of source spectra of the UNE, (2) differences in radiation patterns between the UNE and the earthquake, and (3) influence of high-frequency wave scattering. Here, we examine each factor in turn.

The inaccurate representation of source spectra of the UNE may be direct explanation. As we have previously discussed, the real source spectra of the UNE can be more complicated than expected in the source spectral model, or some portion of energy can be underrepresented. For instance, the high-frequency rolloff rates of UNE source spectra are poorly resolved despite various efforts. The proposed high-frequency rolloff models include f^{-2} (Mueller and Murphy, 1971), f^{-3} (Lay *et al.*, 1984), and f^{-4} (Haskell, 1967). The various UNE rolloff models are reviewed in Denny and Johnson (1991). However, it is well-known that the high-frequency rolloff rates of earthquake spectra agree with f^{-2} (Hanks and McGuire, 1981; Sereno *et al.*, 1988).

If the high-frequency energy from the UNE is underrepresented by the source spectral model, the parameter η of the UNE would be higher than that of the earthquake in all

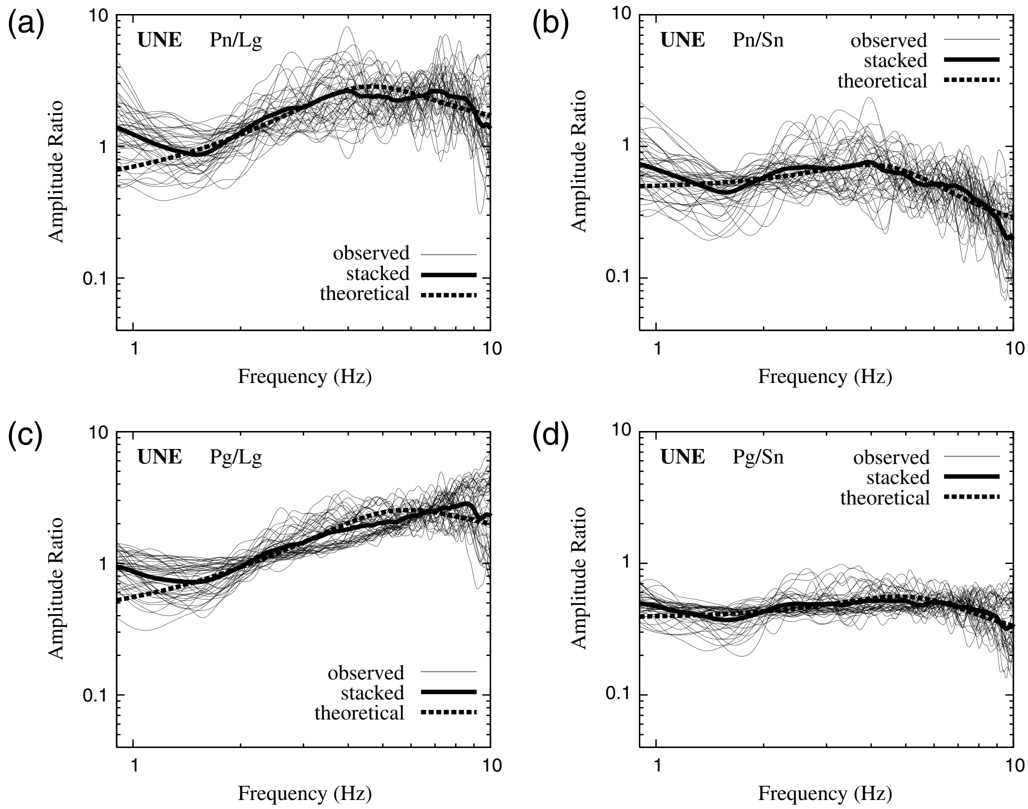

Figure 11. P/S spectral amplitude ratios of the UNE records: (a) Pn/Lg, (b) Pn/Sn, (c) Pg/Lg, and (d) Pg/Sn. The observed P/S spectral amplitude ratios agree with the theoretical curves. The P/S spectral amplitude ratios increase with frequency in the frequencies lower than the P corner frequencies.

ray paths. As shown in Figure 7, the η of Pn and Pg from the UNE is estimated to be higher than that of the earthquake for all stations, although the difference is much reduced in Pg for long-distance stations. Considering that Pn is the mantle-lid P phase and Pg a crustal P phase, the difference reduction in Pg for long-distance stations may be explained with the abrupt crustal-structure variation in the East Sea (Hong *et al.*, 2008; Hong and Kang, 2009).

The influence of the radiation pattern of the sources is another factor to be considered. The radiation pattern of a source causes azimuthal variation in released energy. The azimuth-dependent energy variation can be interpreted as apparent variation of attenuation with azimuth. Thus, the azimuthal variation of the radiation pattern can be a plausible explanation.

The last factor, high-frequency wave scattering, is caused by interference with small-scale heterogeneities in the crust and upper mantle (Capon, 1974; Flatté and Wu, 1988; Sato and Fehler, 1998; Nishimura *et al.*, 2002). Note that high-frequency energy is rich in compressional waves from nuclear explosions. Thus, scattering attenuation of compressional waves is expected to be strong in the high-frequency regime (Hong *et al.*, 2005). The difference in radiation patterns and strong high-frequency scattering may be responsible for the difference in η between the UNE and the earthquake.

In Figures 5 and 6, the relatively high attenuation of regional phases on the paths to the Korean Peninsula may be associated with the Moho undulation and complex crustal transitions due to paleo-continental collisions and rifting (Chough *et al.*, 2000). It is well known that crustal and mantle-lid phases are highly influenced by Moho topography and crustal structures (Kennett, 1986; Kværna and Doornbos, 1991; Zhang and Lay, 1995; Kennett and Furumura, 2001). The influence of crustal structures on regional waveforms from the UNE was confirmed by numerical waveform modeling (Hong *et al.*, 2008).

It is intriguing to note that the Sn phase is less attenuated along paths to the eastern Korean Peninsula than along paths to the western Korean Peninsula, which agrees with an observation in Hong *et al.* (2008). We also find that the LgQ values estimated in this study are lower than those of Hong *et al.* (2008), which are based on a coda normalization technique. This indicates that structural irregularity in the crust causes more significant attenuation than discrete heterogeneities embedded in the crust. This is because much of energy scattered due to structural variations leaks into the mantle. Note that coda waves in local and regional seismograms are mostly composed of energy scattered in the crust. The quality factors from a coda normalization method (e.g., Yoshimoto *et al.*, 1993) reflect the temporal coda-decay rate,

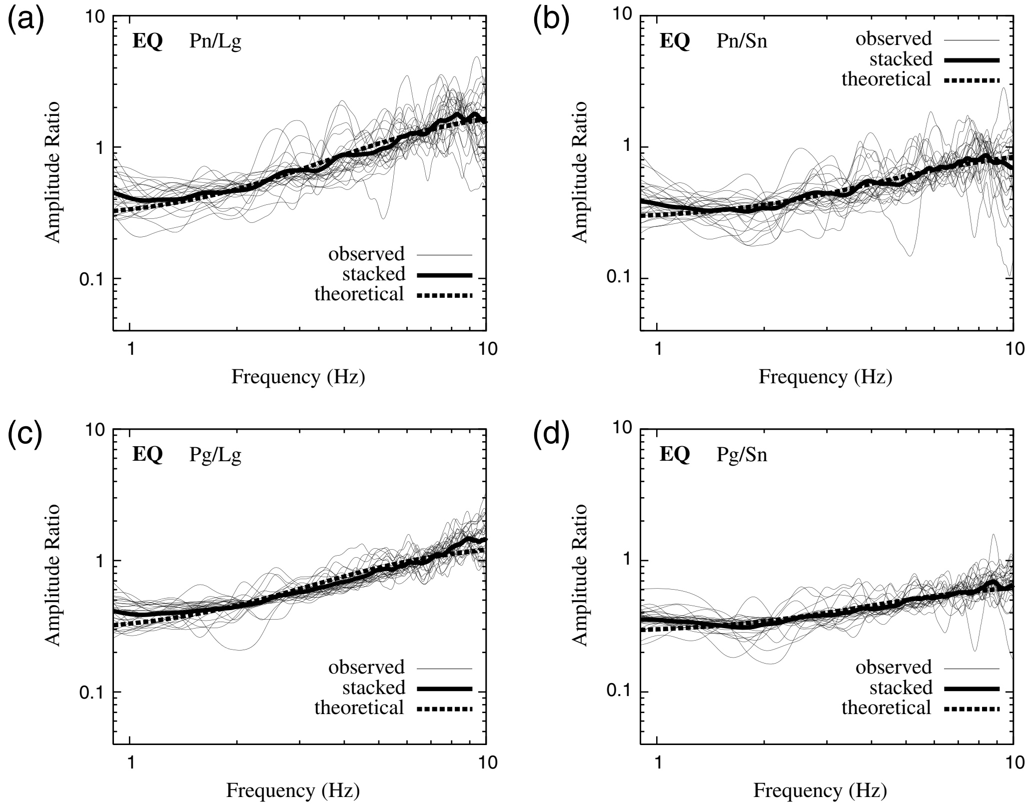

Figure 12. P/S spectral amplitude ratios of the earthquake records: (a) Pn/Lg, (b) Pn/Sn, (c) Pg/Lg, and (d) Pg/Sn. The P/S spectral amplitude ratios increase with frequency.

which does not take account of the amplitude level of the primary wave. The quality factors that we estimated in this study present the actual level of attenuation of the primary wave.

Source Spectrum and the P/S Spectral Amplitude Ratio

The source spectra of regional phases are calculated from equation (5) using the inverted parameters. The inverted source spectra agree well with theoretical expectations for both the UNE and the earthquake (Figs. 9 and 10). The consistent shapes of source spectra at all stations support the stability of the inversion. We observe that the UNE source spectra of Pn and Pg display characteristic overshoot features (Fig. 9). On the other hand, the source spectra of Sn and Lg from the UNE display weak overshoot features.

The spectral amplitude ratios between P and S phases display good agreement with theoretical expectations for both the UNE and the earthquake (Figs. 11 and 12). The P/S spectral amplitude ratios of the UNE increase with frequency in the frequencies lower than the P-phase corner frequencies and decrease with frequency at the higher frequencies. The P/S spectral amplitude ratios of the earthquake appear to increase linearly with frequency in the entire frequency range.

Comparisons of P/S spectral amplitude ratios between the UNE and the earthquake enable us to determine the spectral features of the UNE. The spectral features can be used for discrimination of UNEs from earthquakes. The Pn/Lg and Pg/Lg spectral amplitude ratios of the UNE are well separated from those of the earthquake in the frequency range of 1–8 Hz (Fig. 13). However, the Pn/Sn and Pg/Sn spectral amplitude ratios appear to be less effective.

Characteristics of the UNE Source Spectrum

We have shown that the P/S spectral amplitude ratios are useful for discriminating between UNEs and earthquakes. However, it is not clear whether this is caused by implementation of characteristic UNE source models. We examine the inherent source spectral features of the UNE by testing whether the UNE source spectra can be represented by earthquake source spectral models. We implement Brune's earthquake source spectral model in equation (10) for the test. The source parameters are determined by $M_0 = 2.5 \times 10^{14}$ N m and $f_c = 4.0$ Hz for Pn, $M_0 = 1.5 \times 10^{14}$ N m and $f_c = 5.1$ Hz for Pg, $M_0 = 9.5 \times 10^{13}$ N m and $f_c = 6.1$ Hz for Sn, and $M_0 = 6.5 \times 10^{13}$ N m and $f_c = 2.0$ Hz for Lg (Table 3).

Note that the apparent moments determined from P phases are close to the moment estimated from the low-frequency waveform inversion. Also, these apparent UNE

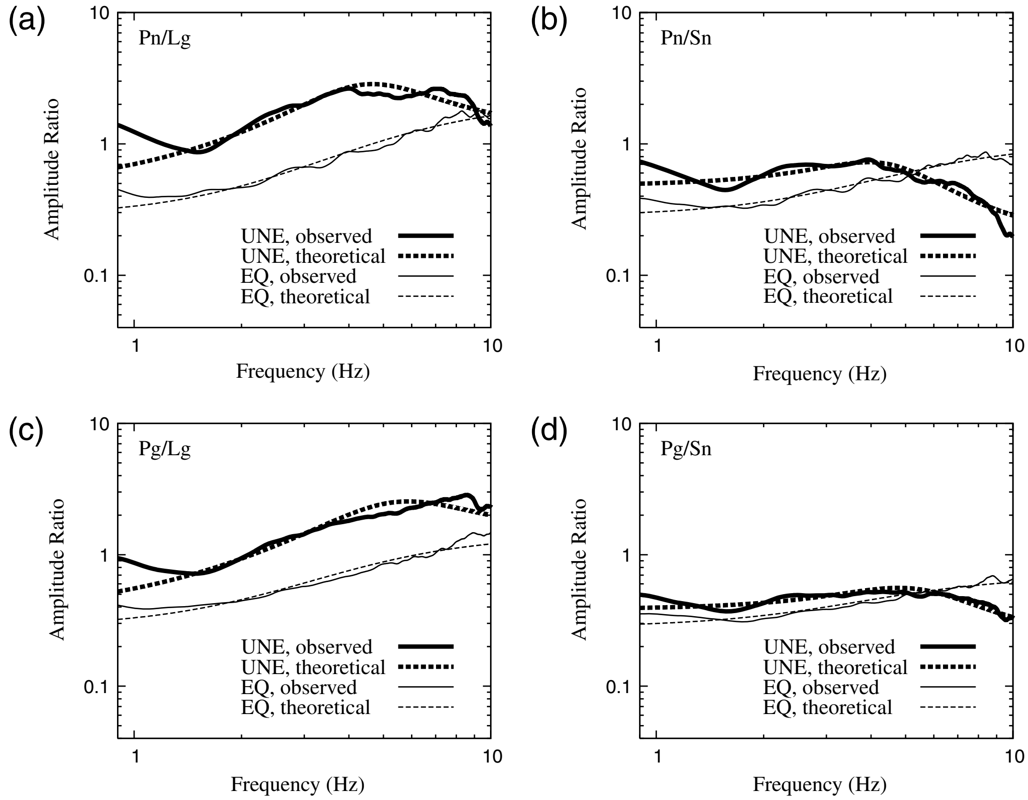

Figure 13. Comparisons of P/S spectral amplitude ratios between the UNE and the earthquake with comparable magnitudes: (a) Pn/Lg, (b) Pn/Sn, (c) Pg/Lg, and (d) Pg/Sn. The P/Lg spectral amplitude ratios of the UNE are well separated from those of the earthquake in the frequency range of 1–8 Hz. The P/Sn spectral amplitude ratios appear to be less effective for discrimination between nuclear explosion and earthquake.

moments are higher than the estimates based on the UNE source spectral models in Table 2. This indicates that the UNE source spectral model appears to underestimate the level of spectral energy compared to the earthquake source spectral model. We also find that the apparent moments for S phases of the UNE are lower than the deviatoric moment of the earthquake. These observations imply that the amount of compressional energy excited from the UNE is similar to that from an earthquake with a comparable magnitude. However, the shear energy from the UNE is far weaker than that from the earthquake.

The source spectra of S phases (Sn, Lg) are reasonably represented by Brune's earthquake source spectral models (Fig. 14). However, P phases (Pn, Pg) are poorly represented due to the characteristic overshoot feature in the P source spectra. Because of the poor representation of P source spectra, the P/S spectral amplitude ratios are poorly matched with the theoretical curves based on Brune's earthquake source spectral models (Fig. 15).

Because the Lg phase is less excited from the UNE than from the earthquake, the Pn/Lg and Pg/Lg spectral amplitude ratios of the UNE display higher amplitudes than those of the earthquake (Fig. 16). The P/Sn spectral amplitude ratios appear to be similar between the UNE and the earthquake. These observations indicate that comparisons of source spectra and shear-energy contents between UNEs and earthquakes of comparable magnitudes may be useful for discrimination of UNEs from natural earthquakes, regardless of the type of theoretical source spectral model adopted.

Discussion and Conclusions

The 9 October 2006 UNE in North Korea was well recorded by dense regional networks deployed in South Korea, Japan, and China. The dense observation allowed us to investigate the regional source properties of the UNE. The isotropic moment of the UNE was estimated to be 2.92×10^{14} N m from long-period waveform inversion. The source spectra of regional phases from the UNE were inverted with

Table 3
UNE Source Spectral Parameters Inverted with Incorporation of Brune's Source Spectral Model

Phase	M_0 (N m)	f_c (Hz)
Pn	2.5×10^{14}	4.0
Pg	1.5×10^{14}	5.1
Sn	9.5×10^{13}	6.1
Lg	6.5×10^{13}	2.0

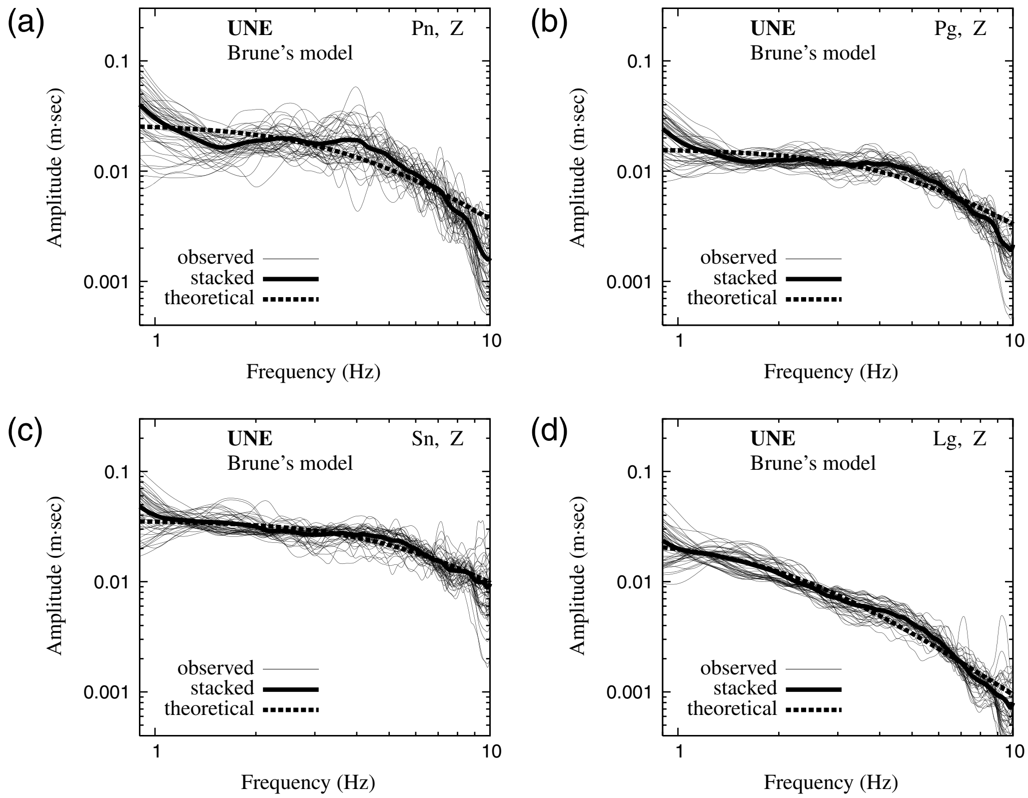

Figure 14. Source spectra of regional phases from the UNE for inversions based on Brune's earthquake source model: (a) Pn, (b) Pg, (c) Sn, and (d) Lg. The P phases (Pn, Pg) poorly match with the theoretical source spectral curves due to the strong overshoot feature. The S phases (Sn, Lg) agree reasonably well with the theoretical curves based on the earthquake source spectral model.

determination of the apparent moments, corner frequencies, overshoot parameters, and attenuation factors. The apparent moments for the regional phases are estimated to be lower than the moment estimate from the long-period analysis, which may be because the source spectra of the UNE are underrepresented by the theoretical source spectral model in low-frequency regime.

The overshoot parameters of P phases from the UNE are higher than those of S phases. The overshoot parameter of Pn is larger than the conventional value, while those of Sn and Lg are lower. The P phases from the UNE are well represented by the UNE source spectral models but poorly by Brune's earthquake source spectral models. However, the S phases for the UNE are well represented by both the UNE and the earthquake source spectral models. These observations suggest that the shear energy may be excited from a secondary source.

Among various shear-wave excitation mechanisms proposed, tectonic release (Wallace *et al.*, 1985), spalling (Day and McLaughlin, 1991), and rock cracking (Massé, 1981) may be plausible. The explosional source features, that is, strong compressional energy and strong spectral overshooting, allow us to use the P/S spectral amplitude ratios to discriminate between nuclear explosions and earthquakes. Such discrimination appears to be effective in the frequency range of 1–8 Hz.

Data and Resources

Event information and seismic waveform data except the UNE data recorded in Korea were collected from the Korea Meteorological Administration (KMA, www.kma.go.kr, last accessed December 2008), the Korea Institute of Geoscience and Mineral Resources (KIGAM, quake.kigam.re.kr, last accessed December 2008), the Incorporated Research Institutions for Seismology (IRIS, www.iris.edu/data, last accessed December 2008), the National Research Institute for Earth Science and Disaster Prevention (NIED, www.fnet.bosai.go.jp, last accessed September 2008), and the International Seismological Center (ISC, www.isc.ac.uk, last accessed December 2008). The seismic waveform data for the UNE recorded in South Korea were collected from KMA and KIGAM with permission.

Some figures were produced using the Generic Mapping Tools (GMT, Wessel and Smith, 1998; gmt.soest.hawaii.edu, last accessed September 2008).

Acknowledgments

We are grateful to KMA, KIGAM, IRIS, and NIED in Japan for making seismic data available. We thank the associate editor, Dr. Anton Dainty, and three anonymous reviewers for their fruitful and constructive comments, which improved the presentation of the article. This work was supported by the Korea Meteorological Administration Research and Development Program under Grant CATER 2007-5111.

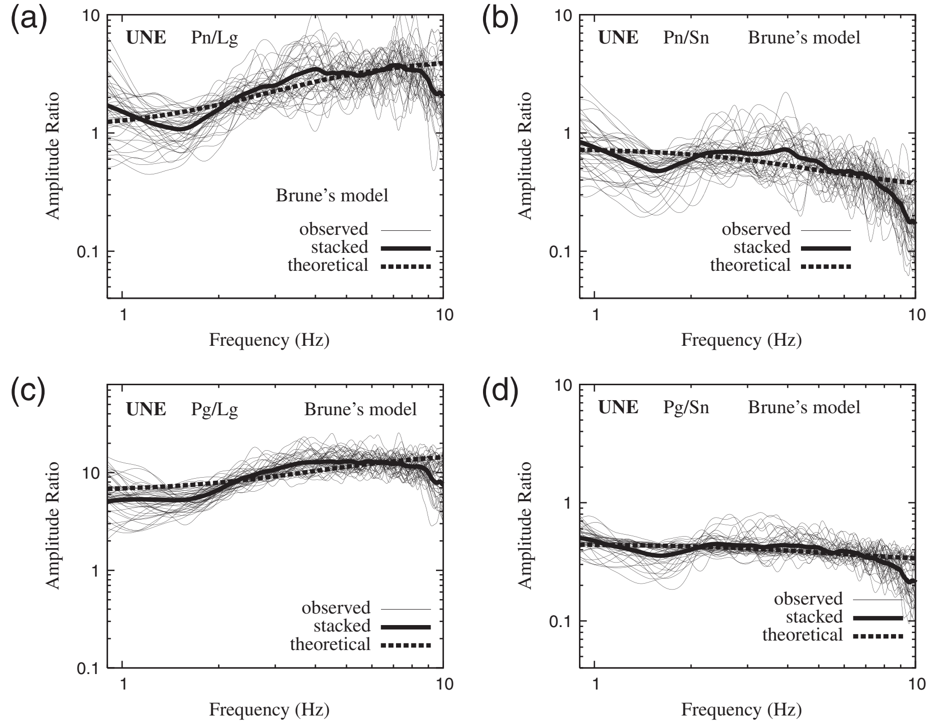

Figure 15. P/S spectral amplitude ratios of the UNE records for implementation of Brune's earthquake source model: (a) Pn/Lg, (b) Pn/Sn, (c) Pg/Lg, and (d) Pg/Sn. The P/S spectral amplitude ratios are poorly represented by theoretical curves based on the earthquake source model due to the characteristic overshoot feature in P phases.

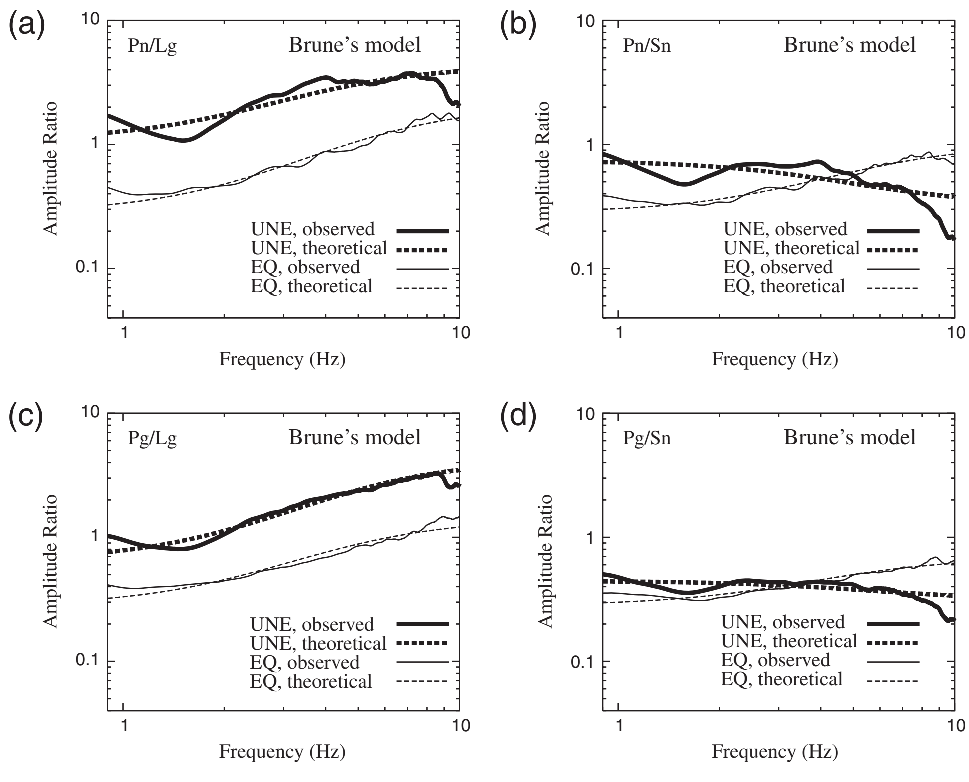

Figure 16. Comparisons of P/S spectral amplitude ratios between the UNE and the earthquake, both of which are inverted using Brune's earthquake source model: (a) Pn/Lg, (b) Pn/Sn, (c) Pg/Lg, and (d) Pg/Sn. The observed Pn/S spectral amplitude ratios of the UNE poorly match with the theoretical curves due to the high overshoot feature in Pn source spectra. The P/Lg spectral ratios of the UNE are well separated from those of the earthquake. The implementation of earthquake source models appears to still be effective for discrimination between nuclear explosions and earthquakes.

References

Aki, K., M. Bouchon, and P. Reasenberg (1974). Seismic source function for an underground nuclear explosion, *Bull. Seismol. Soc. Am.* **64,** no. 1, 131–148.

Aki, K., and P. G. Richards (1980). *Quantitative Seismology, Theory and Methods*, Vol. **1**, W. H. Freeman and Company, San Francisco.

Al-Eqabi, G., K. D. Koper, and M. E. Wysession (2001). Source characterization of Nevada test site explosions and western U.S. earthquakes using *Lg* waves: Implications for regional source discrimination,, *Bull. Seismol. Soc. Am.* **91,** no. 1, 140–153.

Brune, J. N. (1970). Tectonic stress and the spectra of seismic shear waves from earthquakes, *J. Geophys. Res.* **75,** no. 26, 4997–5009.

Capon, J. (1974). Characterization of crust and upper mantle structure under LASA as a random medium, *Bull. Seismol. Soc. Am.* **64,** 235–266.

Chang, S.-J., and C.-E. Baag (2005). Crustal structure in southern Korea from joint analysis of teleseismic receiver functions and surface-wave dispersion, *Bull. Seismol. Soc. Am.* **95,** 1516–1534.

Cho, H. M., H. J. Kim, H. T. Jou, J. K. Hong, and C.-E. Baag (2004). Transition from rifted continental to oceanic crust at the southeastern Korean margin in the East Sea (Japan Sea), *Geophys. Res. Lett.* **31,** 7, L07606, doi 10.1029/2003GL019107.

Chough, S. K., S.-T. Kwon, J.-H. Ree, and D. K. Choi (2000). Tectonic and sedimentary evolution of the Korean peninsula: a review and new view, *Earth-Sci. Rev.* **52,** 175–235.

Chung, T. W., and H. Sato (2001). Attenuation of high-frequency *P* and *S* waves in the crust of southeastern South Korea, *Bull. Seismol. Soc. Am.* **91,** 6, 1867–1874.

Chung, T. W., M.-H. Noh, J.-K. Kim, Y.-K. Park, H.-J. Yoo, and J. M. Lees (2007). A study of the regional variation of low-frequency Q_{Lg}^{-1}, around the Korean Peninsula, *Bull. Seismol. Soc. Am.* **97,** no. 6, 2190–2197.

Day, S. M., and K. L. McLaughlin (1991). Seismic source representations for spall, *Bull. Seismol. Soc. Am.* **81,** 191–201.

Denny, M. D., and L. R. Johnson (1991). The explosion seismic source function: Models and scaling laws reviewed, in *Explosion Source Phenomenology*, Geophysical Monograph 65, S. R. Taylor, H. J. Patton, and P. G. Richards (Editors), American Geophysical Union, 1–24.

Dreger, D. S., and D. V. Helmberger (1993). Determination of source parameters at regional distances with three-component sparse network data, *J. Geophys. Res.* **98,** no. B5, 8107–8125.

Fisk, M. D. (2006). Source spectral modeling of regional P/S discriminants at nuclear test sites in China and the former Soviet Union, *Bull. Seismol. Soc. Am.* **96,** no. 6, 2348–2367.

Fisk, M. D. (2007). Corner frequency scaling of regional seismic phases for underground nuclear explosions at the Nevada Test Site, *Bull. Seismol. Soc. Am.* **97,** no. 3, 977–988.

Flatté, S. M., and R.-S. Wu (1988). Small-scale structure in the lithosphere and asthenosphere deduced from arrival time and amplitude fluctuations at NORSAR, *J. Geophys. Res.* **93,** 6601–6614.

Ford, S. R., D. S. Dreger, and W. R. Walter (2008). Identifying isotropic events using a regional moment tensor inversion, *J. Geophys. Res.* **114,** B01306, doi 10.1029/2008JB005743.

Hanks, T. C., and R. K. McGuire (1981). The character of high-frequency strong ground motion, *Bull. Seismol. Soc. Am.* **71,** 2071–2095.

Haskell, N. A. (1967). Analytic approximation for the elastic radiation from a contained underground explosion, *J. Geophys. Res.* **72,** 2583–2587.

Hong, T.-K., and T.-S. Kang (2009). *Pn* travel-time tomography of the paleo-continental-collision and rifting zone around Korea and Japan, *Bull. Seismol. Soc. Am.* **99,** no. 1, 416–421.

Hong, T.-K., and J. Xie (2005). Phase composition of regional waves from underground nuclear explosions, *J. Geophys. Res.* **110,** no. B12, B12302, doi 10.1029/2005JB003753.

Hong, T.-K., C.-E. Baag, H. Choi, and D.-H. Sheen (2008). Regional seismic observations of the 9 October 2006 underground nuclear explosion in North Korea and the influence of crustal structure on regional phases, *J. Geophys. Res.* **113,** B03305, doi 10.1029/2007JB004950.

Hong, T.-K., R.-S. Wu, and B. L. N. Kennett (2005). Stochastic features of scattering, *Phys. Earth Planet. Interiors* **148,** 131–148.

Kennett, B. L. N. (1986). *Lg* waves and structural boundaries, *Bull. Seismol. Soc. Am.* **76,** 1133–1141.

Kennett, B. L. N., and T. Furumura (2001). Regional phases in continental and oceanic environments, *Geophys. J. Int.* **146,** 562–568.

Kim, W.-Y., V. Aharonian, A. L. Lerner-Lam, and P. G. Richards (1997). Discrimination of earthquakes and explosions in southern Russia using regional high frequency three-component data from the IRIS/JSP Caucasus network, *Bull. Seismol. Soc. Am.* **87,** 569–588.

Kim, S. K., M. S. Jun, and J. K. Kim (1999). Attenuation of *P* waves in the Kyungsang Basin, southeastern Korea, *J. Geol. Soc. Kor.* **35,** 223–228 (in Korean).

Kværna, T., and D. J. Doornbos (1991). Scattering of regional *Pn* by Moho topography, *Geophys. Res. Lett.* **18,** no. 7, 1273–1276.

Lay, T., D. V. Helmberger, and D. G. Harkrider (1984). Source models and yield-scaling relations for underground nuclear explosions at Amchitka island, *Bull. Seismol. Soc. Am.* **74,** no. 3, 843–862.

Massé, R. P. (1981). Review of seismic source models for underground nuclear explosions, *Bull. Seismol. Soc. Am.* **71,** no. 4, 1249–1268.

Mueller, R. A., and J. R. Murphy (1971). Seismic characteristics of underground nuclear detonations, *Bull. Seismol. Soc. Am.* **61,** no. 6, 1675–1692.

Murphy, J. R., and B. W. Barker (2001). Application of network-averaged teleseismic *P*-wave spectra to seismic yield estimation of underground nuclear explosions, *Pure Appl. Geophys.* **158,** 2123–2171.

Nishimura, T., K. Yoshimoto, T. Ohtaki, K. Kanjo, and I. Purwana (2002). Spatial distribution of lateral heterogeneity in the upper mantle around the western Pacific region as inferred from analysis of transverse components of teleseismic *P*-coda, *Geophys. Res. Lett.* **29,** no. 23, 2137, doi 10.1029/2002GL015606.

Paige, C. C., and M. A. Saunders (1982). LSQR: An algorithm for sparse linear equations and sparse least squares, *ACM Trans. Math. Softw.* **8,** 43–71.

Patton, H. J., and W. R. Walter (1993). Regional moment magnitude relations for earthquakes and explosions, *Geophys. Res. Lett.* **20,** 277–280.

Pei, S., J. Zhao, Y. Sun, Z. Xu, S. Wang, H. Liu, C. A. Rowe, M. N. Toksöz, and X. Gao (2007). Upper mantle seismic velocities and anisotropy in China determined through *Pn* and *Sn* tomography, *J. Geophys. Res.* **112,** B05312, doi 10.1029/2006JB004409.

Peppin, W. A. (1976). *P*-wave spectra of Nevada Test Site events at near and very near distances: Implications for a near-regional body wave–surface wave discriminant, *Bull. Seismol. Soc. Am.* **66,** no. 3, 803–825.

Ritzwoller, M. H., M. P. Barmin, A. Villaseñor, A. L. Levshin, and E. R. Engdahl (2002). *Pn* and *Sn* tomography across Eurasia to improve regional seismic event locations, *Tectonophysics* **358,** 39–55.

Saikia, C. K. (1994). Modified frequency-wavenumber algorithm for regional seismograms using Filon's quadrature: Modeling of L_g waves in eastern North America, *Geophys. J. Int.* **118,** 142–158.

Sato, H., and M. Fehler (1998). *Seismic Wave Propagation and Scattering in the Heterogeneous Earth*, Springer-Verlag, New York.

Sereno, T. J., Jr., S. R. Bratt, and T. C. Bache (1988). Simultaneous inversion of regional wave spectra for attenuation and seismic moment in Scandinavia, *J. Geophys. Res.* **93,** no. B3, 2019–2035.

Stevens, J. L., and S. M. Day (1985). The physical basis of m_b:M_s and variable frequency magnitude methods for earthquake/explosion discrimination, *J. Geophys. Res.* **90,** no. B4, 3009–3020.

Taylor, S. R., and H. E. Hartse (1998). A procedure for estimation of source and propagation amplitude corrections for regional seismic discriminants, *J. Geophys. Res.* **103,** no. B2, 2781–2789.

Wallace, T., D. Helmberger, and G. Engen (1985). Evidence for tectonic release from underground nuclear explosions in long period *S* waves, *Bull. Seismol. Soc. Am.* **75,** 157–174.

Walter, W. R., and S. R. Taylor (2002). A revised magnitude and distance amplitude correction (MDAC2) procedure for regional seismic discriminants: Theory and testing at NTS, UCRL-ID-146882, LA-UR-02-1008, Lawrence Livermore National Laboratory, 13 pp.

Walter, W. R., E. Matzel, M. E. Pasyanos, D. B. Harris, R. Gok, and S. R. Ford (2007). Empirical observations of earthquake-explosion discrimination using P/S ratios and implications for the sources of explosion S waves, *29th Monitoring Research Review: Ground-Based Nuclear Explosion Monitoring Technologies*, LA-UR-07-5613, 684–693.

Wessel, P., and W. H. F. Smith (1998). New, improved version of the Generic Mapping Tools released, *EOS* **79,** 579.

Woods, B. B., S. Kedar, and D. V. Helmberger (1993). M_L:M_0 as a regional seismic discriminant, *Bull. Seismol. Soc. Am.* **83,** no. 4, 1167–1183.

Xie, J. (2002). Source scaling of Pn and Lg spectra and their ratios from explosions in central Asia: Implications for the identification of small seismic events at regional distances, *J. Geophys. Res.* **107,** no. B7, 2128, doi 10.1029/2001JB000509.

Xie, J., and H. J. Patton (1999). Regional phase excitation and propagation in the Lop or region of central Asia and implications for P/Lg discriminants, *J. Geophys. Res.* **104,** no. B1, 941–954.

Yoshimoto, K., H. Sato, and M. Ohtake (1993). Frequency-dependent attenuation of P and S waves in the Kanto area, Japan, based on the coda-normalization method, *Geophys. J. Int.* **114,** 165–174.

Zhang, T.-R., and T. Lay (1995). Why the Lg phase does not traverse oceanic crust, *Bull. Seismol. Soc. Am.* **85,** 1665–1678.

Zhu, T., K.-Y. Chun, and G. F. West (1991). Geometrical spreading and Q of Pn waves: An investigative study in eastern Canada, *Bull. Seismol. Soc. Am.* **81,** no. 3, 882–896.

Yonsei University
Department of Earth System Sciences
Shinchon-dong, 134, Seodaemun-gu
Seoul 120-749, South Korea
tkhong@yonsei.ac.kr
(T.-K.H.)

Seoul National University
School of Earth and Environmental Sciences
599 Gwanangno, Gwanak-gu
Seoul, 151-742, South Korea
(J.R.)

Manuscript received 1 April 2008